Powder Technology 409 (2022) 117852

Contents lists available at ScienceDirect

Powder Technology

journal homepage: www.journals.elsevier.com/powder-technology

Photoelastic stress response of complex 3D-printed particle shapes

Negin Amini [a], Josh Tuohey [a], John M. Long [a], Jun Zhang [a], David A.V. Morton [a], Karen E. Daniels [b], Farnaz Fazelpour [b], Karen P. Hapgood [a,c,*]

[a] School of Engineering, Deakin University, 75 Pigdons Road Waurn Ponds, Geelong, VIC 3216, Australia
[b] Department of Physics, North Carolina State University, Raleigh, NC, USA
[c] School of Engineering, Swinburne University of Technology, Melbourne, VIC 3122, Australia

HIGHLIGHTS

- 3D printing photoelastic UV-curable resin enables stress analysis of complex particles.
- Ray tracing confirms shadow at multiple faces of complex particles is from refraction.
- Print orientation affects optical properties of 3D printed discs with applied load.
- Semi-quantitative stress measurement can be obtained from complex 3D printed particles.

GRAPHICAL ABSTRACT

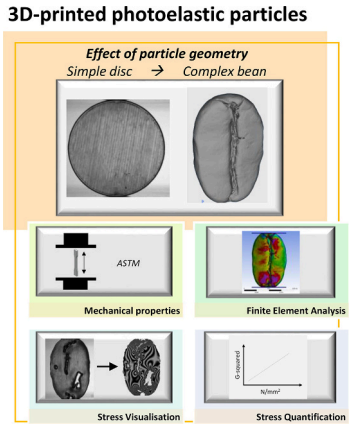

ARTICLE INFO

Keywords:
3D-printing
Particle technology
Finite element analysis
Photoelasticity
Stress visualization
Particle compression

ABSTRACT

Stress visualization within 3-dimensional particles could provide significant insights for understanding of the behaviors of complex particles. However traditional photoelastic methods are only able to produce simple particle shapes. Recently, 3D-printing has created new possibilities for enhancing the scope of stress analysis of physically representative particles. We report the results of X-ray computed tomography and 3D-printing, combined with traditional photoelastic analysis, to visualize strain for particles ranging from simple 2D discs to complex 3D-printed coffee beans, including internal voids. The relative orientation of the print layers and the loading force can affect the optical response of the discs without affecting the mechanical properties. Furthermore, a semi-quantitative measurement of the generated stresses within 3D-printed complex particle is presented. Potential limitations and areas of future interest for stress visualization of 3-dimensional particles are also outlined.

* Corresponding author at: School of Engineering, Swinburne University of Technology, Melbourne, VIC 3122, Australia
E-mail address: khapgood@swin.edu.au (K.P. Hapgood).

https://doi.org/10.1016/j.powtec.2022.117852
Received 5 June 2022; Received in revised form 7 August 2022; Accepted 15 August 2022
Available online 18 August 2022

1. Introduction

Photoelastic methods have been widely used in various experiments to identify regions of stress within single and bulk 2D particle systems [1]. A sample photoelastic visualization is illustrated in Fig. 1: the stress applied to a polymer disc results in an alternating bright/dark fringe pattern when viewed using polarized light. The earliest report of this method being used in the study of granular materials was mentioned in the late 1930s, where it was applied to powdered glass in a Christensen filter [2]. In the 1950s, a report by Wakabayashi applied photoelastic methods to determine the developed stress loads in a powder mass [3]. Currently, this technique has attracted wide attention from the scientific community to deepen the understanding of the internal forces within granular materials, where localized force transmission occurs through structures known as *force chains* [4,5]. The bulk behaviors of real-world particulate matter exhibit similar stress patterns.

To date, quantitative studies [6,7] have largely focused on 2D particle systems, primarily flat discs [8], but also non-spherical shapes such as ellipses [9] and pentagons [10]. While experiments on monolayers of photoelastic spheres can be found in the literature [11–13], interpretations of the resulting fringe patterns remains challenging, even when the system is index-matched. In response to these experimental limitations, there have been advances in computational modelling by using the Finite Element Analysis (FEA) method. This method is capable of efficiently analyzing stress transmission on complex particle systems in a relatively short timeframe [14] a the shapes and forces of deformable particles can also be detected [15].

The underlying mechanism of the photoelastic technique lines in the double refraction of the polarized light incident on transparent polymer, which is sensitive to the local stress along the optical path [16]. The simplest example is considered the photoelastic response for diametric loading on disc shaped particles (see Fig. 1), which has been well established analytically [1]. For discs, the number of observed bright and dark fringes is increased with the force applied to the particle and can be used as a means of calibration for quantitative analysis (Supplementary video 1). The intensity *I(x,y)* at a particular point on the disc can be calculated by using the following eq. (1) [17],

$$I\,(x,y) = I_0 sin^2 \frac{\pi(\sigma_1 - \sigma_2)}{F_\sigma} \tag{1}$$

where (σ_1- σ_2) is the principal stress difference at that point and I_0 is the maximum value of the intensity field. Under monochromatic illumination by light of wavelength λ, the object-specific constant $F_\sigma = \lambda/Ch$ governs the response. Here, the thickness of the flat object is given by *h*, and the material's stress optic coefficient is *C*. It is important to note that when a disc is subjected to 2D stress, the fringe order is proportional to the thickness [1].

The gradient-squared (G^2) method [17] is a semi-quantitative measurement method for quantifying the 2D stress on a particle with an arbitrary number of vector contact forces, developed by Behringer et al.

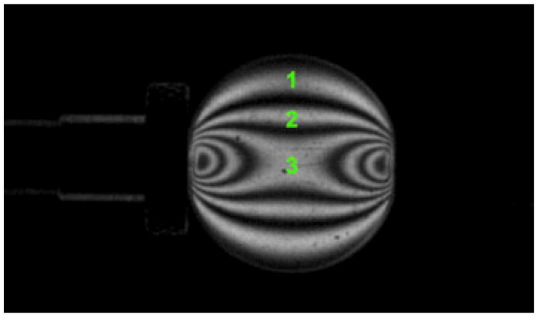

Fig. 1. Illustration of the photoelastic response of a disc subject to diametric load under darkfield configuration with the isochromatic fringes numbered [6].

and collaborators. It is calculated by taking the local (pixel-wise) gradient, squaring, and averaging over all pixels in a particle or system, according to the following eq. (2) [18–21]:

$$G^2 = \sum_{i,j} \Big[\left(I_{i+1j} - I_{i-1j}\right)^2 + \left(I_{ij+1} - I_{ij-1}\right)^2 + \frac{1}{2}\left(I_{i+1j+1} - I_{i-1j-1}\right)^2 + \frac{1}{2}\left(I_{i+1j-1} - I_{i-1j+1}\right)^2 \Big] \tag{2}$$

Although the G^2 method is not based directly on the underlying mechanism of the photoelastic response, it has been widely used for quantifying stresses in granular systems because of its simplicity and ease of calculation [5,20]. More specifically, the G^2 method simply uses the image of the sample or particle being studied, and can also be applied to particles of any shape, including non-circular particles [10]. However, there are challenges in interpreting the results for angular shapes.

Until recently, the majority of photoelastic stress studies have used flat 2D particles because (1) the 2D shapes can be easily machined from flat sheets or cast in molds and (2) discs allow the simplest interpretation of the optical patterns and analytical solutions. Nevertheless, some post-processing treatment is required to remove residual stresses from the material. However, the recent introduction of 3D-printing using photoelastic materials has opened up new possibilities. *Lherminier* et al. [22] investigated the slow shearing of a compressed monolayer composed of 3D-printed discs made on the Objet 30 in Durus White 430 material. The authors were able to successfully reproduced several features of real earthquakes through the dynamic nature of the generated force networks. Wang et al. [23] carried out a comprehensive characterization of the Stratasys commercial 3D-printing material VeroClear, which has photoelastic properties, and was used in standard Stratasys Connex Objet printers [24]. This approach was also employed to 3D print rock-like structures with the aid of x-ray tomography. The internal structure and mechanical response of natural reservoir rocks vary widely due to the sedimentary forming process, and understanding their behavior under stress is important in many geo-mechanical applications [23]. They reported that under triaxial conditions, the samples with horizontal layers have a relatively higher stiffness compared with the vertical layers. However, a small variance was found in the compression strength under different confining pressures. Importantly, in this work, Wang et al. succeeded in reproducing the ratio of the geological stress/rock modulus with a similar lab stress/polymer modulus [23]. Similarly, Ju et al. investigated a 3D-printed rock that contained inherent internal fractures for frozen stress and photoelastic tests. They also reported that the isotropic mechanical properties of the rock sample were comparable to that of the 3D-printed replica rock [25].

The breakage and deformation studies of real particles require either a very large number of samples to be tested, or an acceptance of a relatively large experimental variability and tolerance of uncertainty when interpreting the results. 3D-printing can be used to replicate real particle shapes naturally formed in the environment, as a significant tool for understanding the stress behavior of these complex particles and systems. In addition, 3D printing can create multiple identical copies of real irregular particles that can be used in systematic experimental studies of stress and deformation. As a result, a significant experimental hurdle is overcome. The option to create replica particles with photoelastic materials via 3D-printing permits even more sophisticated experiments to observe stresses for different particles under different stress conditions. Even a small change in the particle shape can significantly affect the stress and photoelastic responses. In the long term, the ability to visualize stress responses in 3D assemblies of complex 3D particles could significantly improve our understanding of particle and agglomerate breakage in industrial applications. Although the development of enhanced models for 3D stress analysis of complex particle systems [25] is some way off, it is worthwhile to investigate what new types of information and analysis can be derived by 3D-printing photo elastic

materials into a more complex 3D particle shape.

In this work, we investigate the photoelastic response of a naturally-occurring complex particle – a 3D coffee bean – including both internal and external surfaces with positive and negative curvature. The presence of internal voids significantly complicates stress visualization, and therefore qualitative and quantitative tests using available methods were also conducted on a modified bean that contained no internal voids. A cross-section of the bean containing the voids was digitally extruded to observe the 2D photoelastic response. We also report the optical and mechanical properties of 3D-printed discs with different alignments of the print layer, compared to a control disc produced via traditional manufacturing methods as a comparative benchmark.

2. Material and methods

2.1. Particle shape construction

The cylindrical disc shape (diameter 20 mm, thickness $h = 10$ mm) was created using Autodesk Inventor CAD software and exported as an *.STL file for 3D-printing.

To reproduce the complex external and internal shape of a coffee bean, X-ray Computed Tomography (Zeiss Xradia 520 Versa XCT) was used to create a volumetric representation of a real coffee bean. This technique records projection images of the x-ray energy transmitted as the sample is slowly rotated 360° in 1-degree increments. The voltage and current required by the x-ray beam [26] are dependent on the sample thickness and material type,. For this work, the optimum contrast of the coffee bean required the implementation of 40 kV and 74 mA for the x-ray beam.

Materialise MIMICS software was used to reconstruct the XCT output DICOM images into a closed surface mesh *.STL file ready for 3D-printing [26]. The original size of the reconstructed coffee bean (11 × 4 × 7 mm) was doubled, and then the rounded ends were truncated to create a flat surface at the top and bottom of the coffee bean shape to assist with handling and applying loads during the compression testing. Three versions of this coffee bean particle were investigated; namely one containing its internal void structure, another simplified version with internal voids removed, as well as a 2D extruded cross-section of a slice of the bean with internal voids.

2.2. Particle materials

The 3D-printed particles were produced by using Stratasys VeroClear UV-curable polymer, an acrylate-based photopolymer. This material was selected because it is the only commercial 3D printing material with photoelastic properties compatible with our Stratasys Connex 3D printer.

For this work, the mechanical properties were experimentally measured by using the ASTM D638 standard tensile and ASTM D695 standard compression tests, and the respective data are summarized in Table 1. The tensile specimen of Type-I design for the yield and tensile strengths and the standard compression cylinder specimen design for the elastic modulus were used [27,28]. Three orientations for the build of the tensile specimen and two orientations for the compression specimen on the 3D printer were also investigated. Fig. 2 shows the position of each specimen on the platform so that the print layers are parallel (Fig. 2A and D) or perpendicular (Fig. 2B, C and E) to the platform when they are when in the upright orientation. These tests measured the impact of the print layer orientation on the mechanical properties and provided material constants for use in the FEA analysis.

Table 1
Material mechanical properties of VeroClear and Acrylic generated according to the ATSM D638 and D695 standards and values reported in the literature.

VeroClear	Specimen (Fig. 2)	Elastic Modulus (MPa)	Poisson's ratio
ASTM D638 standard tensile test	S1	3028 ± 112	–
	S2	2788 ± 124	–
	S3	2953 ± 102	–
ASTM D695 standard compression test	S4	2586 ± 14	–
	S5	2591 ± 21	–
Simulation data		2500	0.38
VeroClear§		2000–3000 [24]	0.38 [25]
Acrylic§		3300 [30]	0.38 [31]

§ Literature values.

2.3. 3D-printing of particles

A Stratasys Objet500 Connex3 3D printer was used to additively manufacture VeroClear particles by using the polymer jetting method. This process involved selective jetting and polymerization of a photopolymer resin to build up the layers of a 3-dimensional object. Input geometry *.STL files were prepared for printing by using the Objet Studio slicing software to set build parameters and generate support structures. High-quality 16 μm layers at an XY-resolution of 600 DPI were specified. The compatible water-soluble support material was also used to support overhanging regions and any internal voids; while this material was removed in the post-manufacture processing. In samples with internal voids, a small amount of support material was fully encapsulated within the internal voids and could not be removed. This was considered to have negligible impact on consequent test results as reported in other studies [23,25]. Sample particles were also printed without containing internal voids (i.e. completely solid) to eliminate this minor effect.

Flat discs were also 3D-printed in the same manner as the ASTM compression standard specimens to determine whether the orientation of the print layers can affect the optical properties of the particle. One disc typically takes 33 min to print in high-quality mode and requires six grams of material and two grams of support material. When multiple discs are printed simultaneously the machine requires less time: for example, 44 discs require two hours to print. Similarly, each coffee bean requires four grams of print material and two grams of support material and the printing process takes 35 min to complete. On the contrary, one hour is required to print 40 beans.An Olympus SZ61 DP22 microscope was used to capture images of the resulting particles.

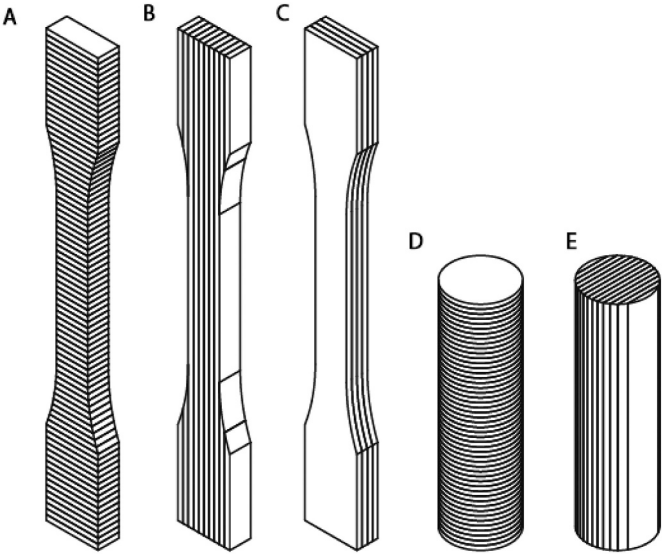

Fig. 2. Schematic illustration of the print layers' arrangement for each specimen tested. (A) Tensile specimen - S1 (B) Tensile specimen - S2 (C) Tensile specimen - S3 (D) Compression specimen – S4 and (E) Compression specimen - S5.

2.4. Laser cutting of disc particles

The control particles were laser cut from 10 mm sheets of PMMA (polymethyl methacrylate) by using a Trotec Speedy 500 laser cutter with a 120-W CO_2 laser. Adobe Illustrator was used to create the 2D profiles, which wereexported as .DXF files for input to the laser cutter.

2.5. Instron compression of particles using the circularly polarized light configuration

For our polariscope, a brightfield configuration was used: two circularly polarizing filters (CIR-PL), both with the same chirality, were placed on either side of the sample (Fig. 3). Each CIR-PL filter comprised a quarter-wave plate on the side facing the particle, in series with a linear polarizer on the other side. Moreover, an opaque acrylic sheet was placed between the monochromatic sodium lamp (wavelength of 589 nm) and the first CIR-PL for uniform lighting.

Individual particles were also placed between the steel plates on an Instron 5959 electromechanical universal test machine (50kN load cell). A strain rate of 1 mm/min was applied, up to a maximum displacement of 2.0 mm. Three specimens of each type were individually tested, while the load and displacement were recorded at a rate of 10 Hz.

The acquired images (TIFF, 2048 × 2048 pixels) were recorded with a PCO.edge 4.2 monochrome high-speed camera with a rolling shutter at 10 frames per second. In addition, a black acrylic cage with two holes for the placement of the filters was placed around the compression plates for two reasons. First, as a safety measure to prevent flying shards in the instance of particle compression failure. Second, to restrict non-polarized light from interfering with the imaging process.

2.6. Gradient-squared (G^2) method for semi-quantification of 2D stress on system

The MATLAB Image Processing Toolbox was used to segment the TIFF images and isolate the foreground particle from the background and calculate the G^2 value (Eq. 2) on the visible stress fringes. The G^2 method was applied to the control disc and all the 3D-printed particles in both 2D and 3D. These values were then plotted against the corresponding measured test load, with the load normalized by the average cross-section area perpendicular to the load direction. For the disc, the load was divided by the average cross-sectional area perpendicular to the loading direction. This was performed analytically to get an average area. For the coffee bean, (both cross-section and 3D variants) the load was divided by the average cross-sectional area of a finite number of intersecting planes.

2.7. Finite-element analysis of the particle compression

To visually validate the observed experimental stress fringes for the disc and the 2D extruded bean cross-section, Finite Element Analysis (FEA) was applied. Quasi-static 2D plane stress FEA was conducted on the particles in ANSYS Workbench, using the static structural analysis system. The VeroClear material was modeled as isotropic and linearly elastic, with modulus 2500 MPa and Poisson ratio 0.38. The ANSYS Mechanical application was employed to generate finite element meshes and set up the analysis system, replicating the Instron compression test configuration. The external loads were applied by using zero-slip contacts with flat rigid plates, the lower plate was fixed and the upper plate was driven with a ramped displacement of 2 mm. The solutions were obtained by using the default MAPDL (Mechanical Ansys Parametric Design Language) solver and the Newton-Raphson method to account for geometric non-linearities that are associated with contact models and large deformations.

A mesh convergence study was performed to monitor the reaction force at the displacement boundary conditions and a mesh-independent solution was found for uniformly-sized second-order quadrilateral elements (maximum nominal size of 0.125 mm for the cylinder and 0.25 mm for the bean cross-section). To strike a balance between mesh-independence and solving time, 0.15 mm and 0.2 mm elements were used for the cylinder and digitally extruded bean cross-section, respectively. Additional refinement was added around regions with large stress gradients.

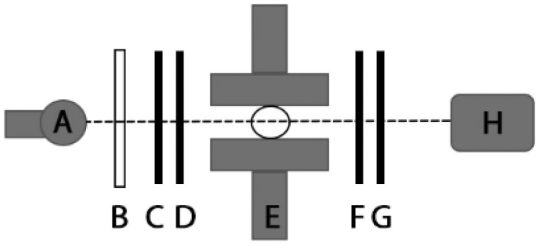

Fig. 3. Schematic illustration of a circularly polarized light with a brightfield configuration set up around the Instron. A. Monochromatic sodium lamp, B. Light diffuser (acrylic sheet), C. Linear polarizer, D. ¼ wave plate, E. compression plates, F. ¼ wave plate, G. Linear polarizer, H. Camera recorder.

2.8. Eliminating the 3D-printed coffee bean shadows

The Autodesk Maya software was used to construct a virtual representation of the polariscope test environment, by using reference images to approximately match lighting, material, and camera setup. The Monte-Carlo based renderer Arnold was then used to render the extracted images of test specimens placed within a medium of the refractive index of $n = 1$ (air) or $n = 1.52$ (index-matched to particle) on the initial unloaded appearance of the specimens. The rotation of the polarization due to the waveplate-like behavior of acrylic was not accounted for.

3. Results and discussion

3.1. Stress visualization of a 3D-printed disc

The photoelastic response of cylindrical discs was systematically examined to test the potential existence of any optical effects arising from the layers created by the 3D-printing process. The same measurements were performed on a control disc, which was laser cut from a solid acrylic sheet. Both materials possess photoelastic properties. The images of the 3D-printed and laser cut discs before compression in natural light are shown in Fig. 4A and B, respectively. The laser-cut disk is transparent, as expected, but the layers cause the 3D-printed discs to be slightly translucent. Interestingly, the irregular surface visible on the 3D-printed disc was caused by the removal of supporting material, and is visually enhanced by the camera flash. The application of a post-processing of the surface with sandpaper would minimize the visual appearance, if necessary. However, this was not necessary for these experiments as it did not affect the photoelastic response.

One potential limitation of polymer 3D printing is the inherent anisotropy of 3D-printed particles due to the layer-based photo-polymerization building process. These layers could potentially lead to different optical and mechanical properties based on the print layer orientation and shape of the particle under compression. It is possible that there might be a range of properties for a given 3D-printed particle, since the microstructure of the 3D printed part due to layer-wise deposition would be different based on the orientation of the particle relative to the imposed compression. Fig. 5 depicts the particle build positions on the 3D printing platform and a schematic of the particle layer orientations between the compression plates.

The orientation shown in Fig. 5A comprises of 1250 layers stacked in the direction of the height of the disc (20 mm), whereas Fig. 5B displays half the number of layers stacked to make the thickness of the disc (10

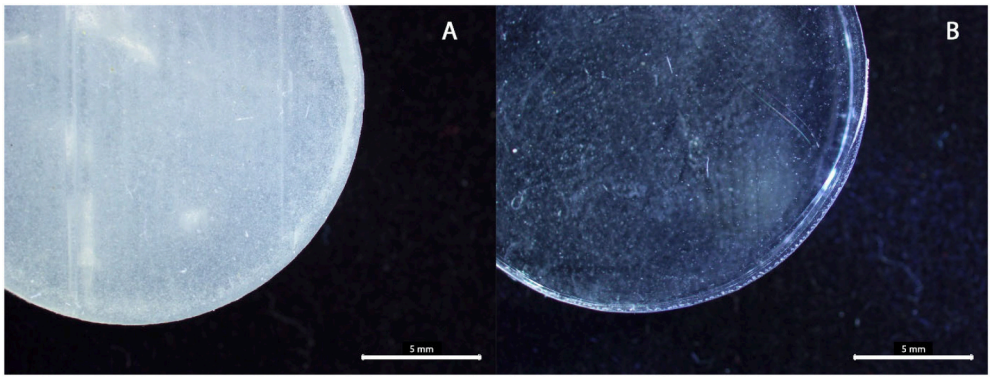

Fig. 4. Image of the discs (dimensions: thickness 10 mm, diameter 20 mm) procured by two different methods (A) 3D-printed in VeroClear and (B) laser cut from acrylic sheets.

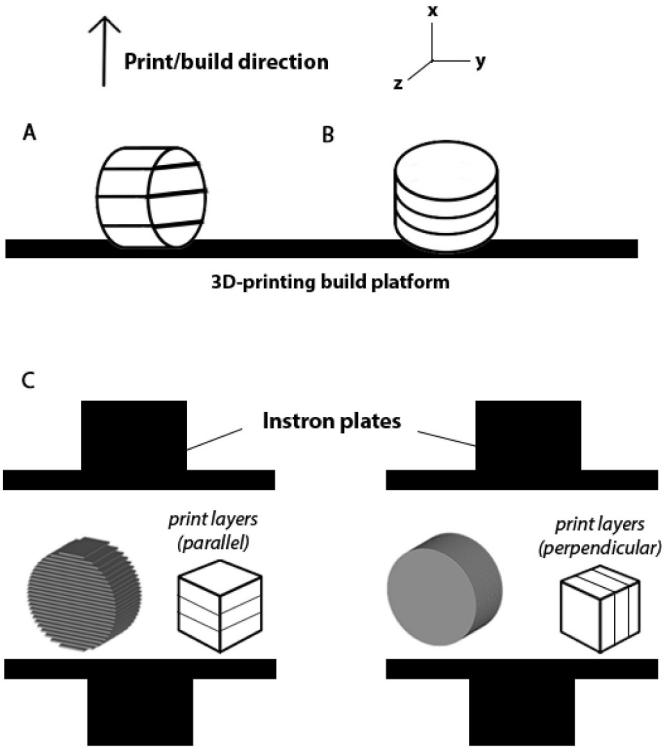

Fig. 5. Schematic illustration of the particle orientations and the direction of build on the 3D printer platform showing (A) parallel and (B) perpendicular print layers when the discs are in the upright position. (C) Depiction of the Instron setup showing the particle print layer arrangement with respect to the compression plates.

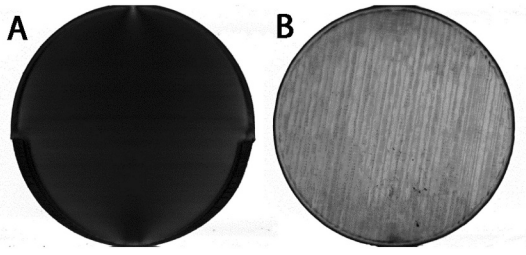

Fig. 6. Image of an unloaded disc viewed through the brightfield configuration with print layers (A) parallel and (B) perpendicular to the compression plates.

mm). When the particles were placed between the compression plates, they were viewed through a *brightfield* setup.

Fig. 6A shows the image of an unloaded particle with parallel print layers, starting off *dark* prior to compression. In contrast, Fig. 6B reveals the image of an unloaded particle with perpendicular print layers which starts off light, as was expected to be observed with a brightfield setup. The acrylic-based polymers (such as VeroClear) act as optical waveplates and rotate the polarization of light, unlike the materials that are typically chosen for photoelastic materials (but which cannot be 3D-printed). This rotation, in combination with the microstructure arising from the two different print layer orientations, makes the resulting discs differ in their optical response even when they are unloaded. If these particles were used for quantitative force measurements, it would be necessary to account for this baseline optical rotation by using a calibrated waveplate, specific to the chosen print-orientation and particle thickness [1]. The stripes observed on Fig. 6B arise from the pattern formed by the 3D-printing nozzle traversing across the printing surface to draw the top layer of the disc and are not the layers themselves.

To simplify the issue of anisotropy, only four discrete orientations were explored to examine whether there is an impact on the optical properties of 3D-printed discs during compression. The top row of Fig. 7 illustrates these four orientations with the placement of all discs (3D-printed and control) as they were placed between the compression plates.

The middle row in Fig. 7 shows the very first recorded isochromatic fringe ($N = 1$) that was observed for each disc. The alignment of the first fringe with respect to the applied diametric contact force is varied for each of the 3D-printed discs, due to the relative orientation of the layers and the loading axis. The 3D-printed disc with printed layers perpendicular to the steel plates (Fig. 7D) shows a dark stress fringe, which is comparable to the control disc (Fig. 7E). The disc with parallel layers (Fig. 7.A) also shows the first recorded bright fringe to be similar. However, the outer edge of the disc contains an uncharacteristic silhouette partly due to the further rotation of the light's polarization and the print layer orientation. Furthermore, Fig. 7B and C show a slightly distorted/skewed first recorded bright fringes, as well as an additional uncharacteristic silhouette on the outer edge. Based on these observations the more complex coffee bean shape was selected to be printed so that all the layers were perpendicular to the steel plates, to minimize additional fringe distortion.

The bottom row in Fig. 7 shows all discs with 5 fringes ($N = 5$). The shape of the bright/dark bands appeared to be the consistent with what has been reported in the literature [6]. Force measurements were taken for $N = 5$ fringes to check whether the shape of the particle has a significant impact on the material properties. A summary of the force load (*Newtons*) and displacement (*mm*) that are required to reach $N = 5$ fringes is given in Table 2. The control disc reached this point by applying almost three times higher force load than the 3D-printed discs,

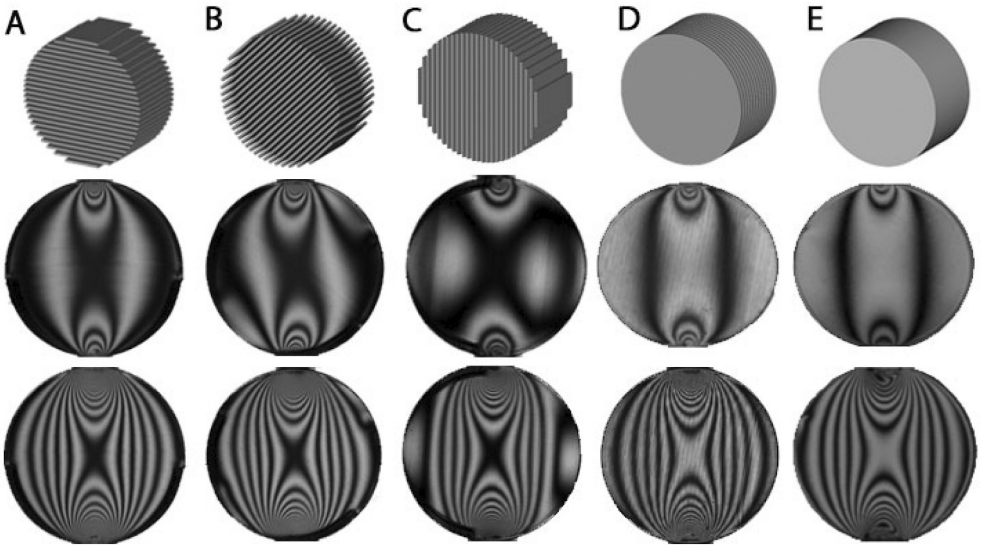

Fig. 7. Top row – 3D representations of the discs to show print layer orientation with respect to the steel plates (A) parallel - 0° (B) parallel - 45° (C) parallel - 90° (D) perpendicular and (E) isotropic. Middle row – Images of the first recorded ($N = 1$) isochromatic stress fringe observed for each respective disc. Bottom row - Images of the fifth (N = 5) isochromatic stress fringe observed for each respective disc.

Table 2
Experimental data for the force load measurements that were taken directly from the Instron for 5 isochromatic fringes (N = 5). The compressed discs 3D-printed in VeroClear (parallel & perpendicular layers) and for the control disc. Comparative FEA data for VeroClear.

	Disc shape (Fig. 6)	Force Load (N)	Displacement (mm)
3D-printed material – VeroClear			
Parallel	A, B, C	1419 ± 73	0.3 ± 0.02
Perpendicular	D	1542 ± 34	0.3 ± 0.02
FEA		1666	0.2
Laser cut material – Acrylic			
Isotropic	E	4809 ± 106	0.8 ± 0.04

due to its stiffer material properties. Notably, the force required for the 3D-printed discs to reach $N = 5$ was consistent regardless of the printed layer alignment. This is further discussed in Section 3.2 with the FEA data. For the discs with parallel print layers (Figs. 7A, B and C), the shape of the bright/dark bands on the outer edge of the discs was pushed further to the edge with each addition of more fringes. This effect is not consistent with the expected behavior for isotropic, elastic materials.

Visualization of the stress fringes over increasing force loads permitted calibration of the materials for calculation of the stress optic coefficients (C). Following the approach of Daniels et al. [7], Fig. 8 plots the normalized force load with respect to the disc diameter (kN/m) against the first six isochromatic stress fringes observed on the discs. The contrast between the sensitivity of the optical properties for the two materials are clearly shown as approximately 150 kN/m was required to achieve five fringes for the 3D-printed discs. In contrast, almost 500 kN/m was required to achieve the same number of fringes for the acrylic discs. By using 3D-printing, the stress optic coefficient was significantly lowered from its isotropic value. The C value in Fig. 8 was calculated by using the gradient of the normalized force at a wavelength of $\lambda = 589$ nm.

Fig. 7 also shows that while the pressure at which the first recorded stress fringe appears depends on the choice of print direction and the relative orientation with respect to the compression plates, from the calibration (Table 2) it was demonstrated that the mechanical force required remains consistent [24]. VeroClear is an acrylate-based UV curable resin, which deforms like a ductile material [23]. Manufacturer

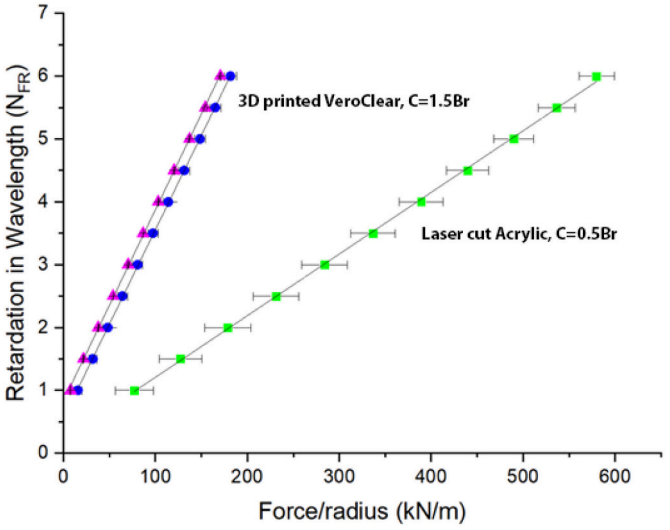

Fig. 8. Graph for the calibration of F_α for the discs in VeroClear and acrylic materials. The 3D-printed disc: VeroClear with 'parallel' Δ (average taken for 0°, 45° and 90°) and 'perpendicular' ∘ print layers with respect to the compression plates. The laser cut disc: Acrylic □.

formulations are subjected to the alteration from time to time, and as a result, a recalibration of the stress-optic coefficient is advised for each new batch.

3.2. Finite element analysis of the disc stress visualization

ASTM tensile and compression tests on the VeroClear were conducted to determine the mechanical properties of the VeroClear material for the FEA model parameters. Table 1 summarizes the material values generated for VeroClear in this work. A minimal difference in the elastic modulus with respect to print layer orientation was measured. Similar findings were reported by Bass et al. [29], where the mechanical properties of one rigid and one flexible polymer from the Stratasys Vero material range in three print orientations were investigated. The authors reported minimal difference in the elastic modulus for the rigid material VeroWhitePlus as a function of the print orientation. In contrast, a

significant difference in the elastic modulus of the elastic material TangoBlackPlus in one of the investigated print orientations was detected. Objects printed with VeroClear and VeroWhite are strongly bonded in all directions, including the interstitial layer boundaries, and the 3D-printed objects are no longer sensitive to print orientation.

Since the optical behavior of the perpendicular printed disc was similar to the behavior of the control disc (an isotropic material), the FEA model of the 3D-printed particles was treated as an isotropic material. For the disc shape, the principal stress fields from the stress-optic equation were used to visualize the stress fringes in FEA. It is quite important to note that FEA produces an isosurface mesh, which means that the visualized regions of stress apply only to the surface being viewed. Due to the 2D shape, the principal stress remained constant through the cross-section. Fig. 9 shows the visual evolution of the FEA disc commencing from a mesh representation, through to the final gradient intensity.

Table 2 compares the experimental and computational data for the 2D disc at $N = 5$. The load requirement and displacement that were needed to obtain $N = 5$ in the FEA simulation were in good agreement with the experimental data. The slight discrepancy between the force load from the experiment and the FEA could be accounted for the simple linear elastic model that was used for the material in the FEA, since the compressions were performed at small displacement. A model that takes into account more complex material properties and deformation of the disc is likely to produce results closer to the experimental data.

Fig. 10 illustrates the first recorded isochromatic stress fringe ($N = 1$) for the 3D-printed disc with parallel orientation of 45° to the compression plates, for both the experimental and FEA data. The asymmetrical fringe pattern exhibited by the 45-degree rotated specimen was of particular interest, as this behavior could not be replicated in the FEA simulations by using the linear isotropic material model (circled in red in Fig. 10B). Implementing a 2D orthotropic model in FEA and significantly decreasing the elastic modulus in one axis (to mimic the variation in the strength depending on the 3D-printed layer direction) a similar asymmetric pattern was produced. However, this anisotropic material model conflicts with the experimental test data, and lacks an accurate shear modulus value. A more detailed investigation into the anisotropic material properties and their impact on the photoelastic properties was beyond the scope of this work.

3.3. Stress visualization of complex 3D-printed shape

Fig. 11 shows the image of (Fig. 11A) the real bean, (Fig. 11B) the computer-aided model of the bean and (Fig. 11C) the final 3D-printed bean in VeroClear. The 3D-printed coffee bean samples were then compressed in the upright position (bean line perpendicular to the steel plates). Although the compression of the bean on its side (bean line parallel to the steel plates) was possible, the experiments were less repeatable due to instabilities caused by the irregularity of the shape. Subsequently, the coffee bean designs were 3D-printed in the perpendicular orientation (as shown in Fig. 7D) in order to minimize the

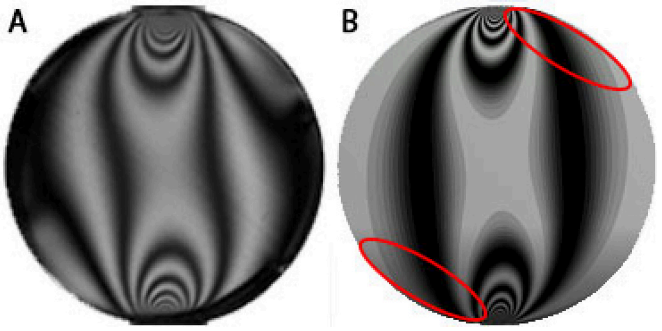

Fig. 10. Image of the particle under load to give N = 1 for (A) 3D-printed disc with parallel layers at the 45° orientation and (B) the disc in the FEA with the transversely isotropic material model. Parameters used: Orthotropic linear elastic material. Elastic modulus 1: 1500 MPa, Elastic modulus 2: 3000 MPa, Poisson ratio: 0.38, Shear modulus: 800 MPa. The element coordinate system is oriented 45° from the horizontal. Red circles highlights where FEA simulation (B) did not capture the asymmetric fringe pattern shown in the experiment (A). (For interpretation of the references to colour in this figure legend, the reader is referred to the web version of this article.)

influence of the anisotropic photoelastic response.

Some dark patches within the photoelastic response of the unloaded 3D-printed coffee bean were observed. On the contrary, no obvious stress fringes were detected for the bean particles with voids due to the complexity of the 3D shape throughout the cross-section. However, stress fringes were clearly visualized in a solid particle by using the existing methods for 2D and pseudo-2D particles. This shadow-like effect could be eliminated by surrounding the particle with suitable media of matching refractive index (n). This hypothesis was validated by carrying out in silico ray tracing experiments of the uncompressed particle, whereas a ray was passed through the particle with matching and non-matching n, respectively. Media with matching n media can also eliminate the shadow. The shadow was caused by refraction at the multiple faces of the complex shape and not by frozen internal stress, as this effect was not observed in the 3D-printed discs. Fig. 12 shows the existence of ray-traced images of the uncompressed coffee bean (with and without internal voids) in a surrounding environment with from matching (left) to non-matching (right) refractive index to the particle. It is interesting to notice the existence of a dark patch at the outer edge of both 3D-particles with a non-matching refractive index. The shadow on the outer edge of the 3D particle produced by the mis-matched refractive index wss a lensing effect.

FEA simulations were also performed for the compression of the coffee bean, as shown in Fig. 13, with internal voids displaying the Von Mises stress at 0, 1 mm and 2 mm displacement. Furthermore, slices at intervals of 1 mm were extracted to show the stress distribution through the whole bean. The intensity can then be determined at any point in the FEA for comparison to the experimental response. However, the direct comparative experimental setup could not be carried out due to the

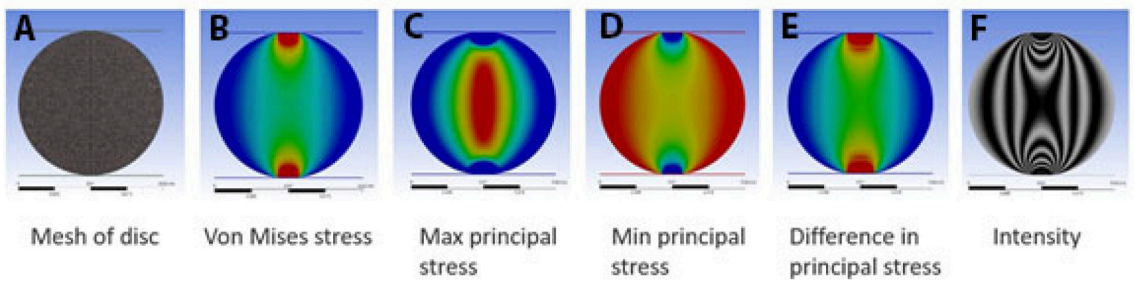

Fig. 9. Evolution of the FEA disc (A) Mesh of the disc (B) Von Mises stress (C) Maximum principal stress (D) Minimum principle stress (E) Difference in principle stress (F) Intensity.

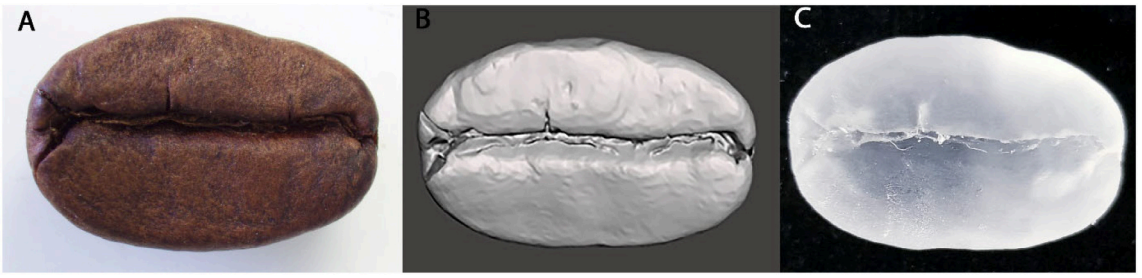

Fig. 11. Image of (A) real coffee bean (B) CAD model of coffee bean and (C) 3D-printed coffee bean. Dimensions of (A) 11 mm length, 4 mm thickness and 7 mm height and (B, C) 22 mm length, 14 mm width and 8 mm thickness.

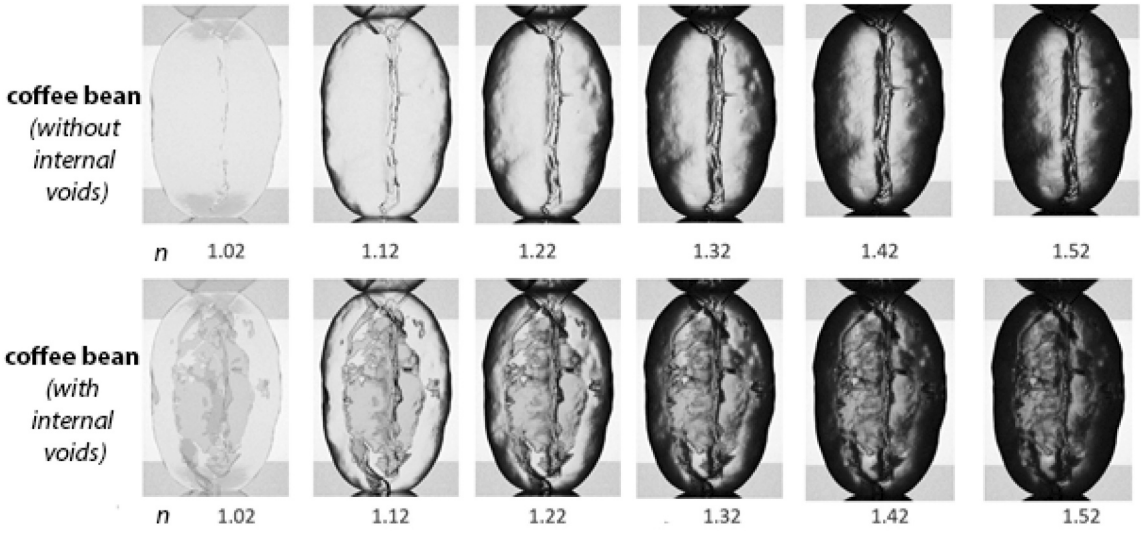

Fig. 12. Ray tracing images of uncompressed coffee bean; Top row – without internal voids, Bottom row – with internal voids; surrounded by (left) media with matching refractive index through to (right) media with non-matching refractive index (same as the experiment).

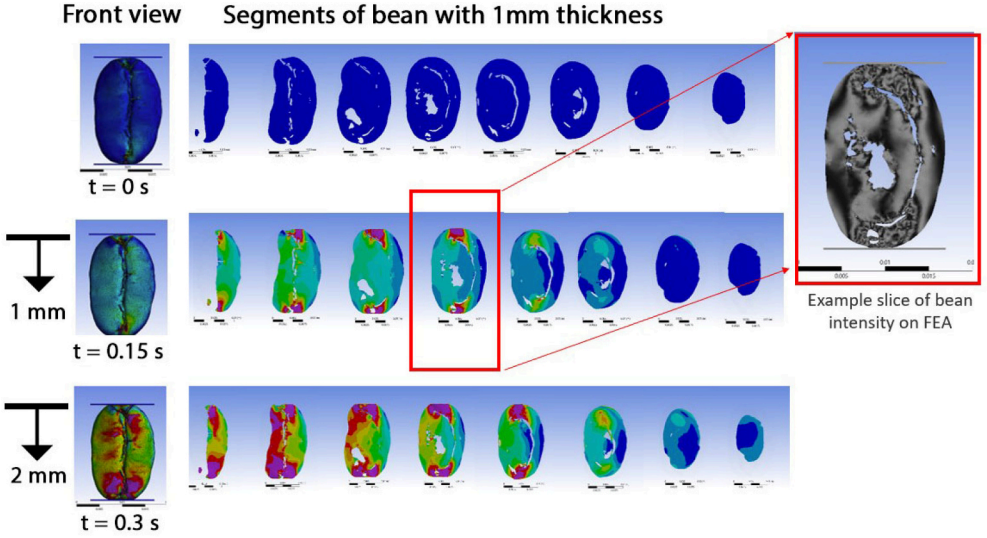

Fig. 13. FEA compression for the coffee bean with internal voids at 0, 1 and 2 mm displacement. Segments were taken at every 1 mm throughout the whole bean starting from (left hand side) the front of the bean to (right hand side) the back of the bean.

instability of the bean at such fine measurements.

In one prior study, an X-ray CT scan of a soil sample with inherent internal fractures was compressed under conditions, which captured and locked in the internal stress [32]. By using this technique, slices through the cross-section could be taken of the experimental sample after compression and directly compared to the FEA. It is quite important to note that the sample was a stable shape which could be kept upright without modification to the design or support. Therefore, to try to observe the photoelastic response inside the bean with the internal voids, a planar cross-section of the bean particle was extracted and

digitally extruded to 10 mm thickness for 3D printing. This was done to deepen the understanding during the formation of stress fringes around the voids.

For a cross section of the coffee bean with internal voids, the experimental photoelastic response was compared against the FEA intensity. Fig. 14A shows the experimental photoelastic compression of the bean slice at a low displacement. From the comparative 2-Dimensional FEA analysis of the digitally extruded cross-section, good agreement with respect to the formation of isochromatic fringes was demonstrated, particularly in regions of high stress around the voids (Fig. 14B). Additionally, compression of the particle eventually led to particle fracture.

3.4. Stress quantification of 3D-printed particles by using the gradient-squared method

There have been a few reports on the stress quantification of complex shaped particles [11,13,32]. The addition of complex internal voids has not been considered in these methods. Currently there are no solutions to this problem. The gradient squared method (G^2) is regarded as a method which could be used for such particles as it has proven successful in a variety of circumstances. It is an approach which has been used to measure the empirical 2D stress of particles (mainly discs) by quantifying the sum of the squared gradient of the light intensity produced over increasing force loads. Although this method has been used for studying the stress birefringence of granular packing in 3 dimensions [11], it has never been applied to 3D-printed particles of complex or porous geometries. The presence of bright voids would need to be excluded from the G^2 analysis to be meaningful. This would be possible with image segmentation.

Semi-quantitative stress measurements have been applied to conventionally flat, but non-circular, particle shapes by Zhao et al. [10], and a similar analysis was performed here. Fig. 15 presents the plot of the G^2 produced from the compression videos of the particles against the respective normalized force loads. The extracted G^2 value is much higher for VeroClear compared to the acrylic material, presumably due to the difference in the stress optic coefficient that was reported above.

The G^2 value grows linearly with the applied load (Fig. 15D) as expected with this method [5,8]. The G^2 value for the 3D-printed 2D disc shapes (Figs. 15A & C) increases linearly with the applied load, once the load is above approximately 3 MP before reaching a plateau. The initial deviation in the trendline below 3 MPa could potentially be due to asperities on the unpolished particle surface or compression stage, with the particle shifting position during the early stages of compression. As the strain on the 3D-printed discs increased, larger deviations in the G^2 value were recorded, which could be due to the material plastically deforming (making the observations not reversible as the load is decreased). This effect suggests that there is a window for meaningful stress interpretation at low loads, before it begins to slightly plateau and ultimately deviate at higher loads.

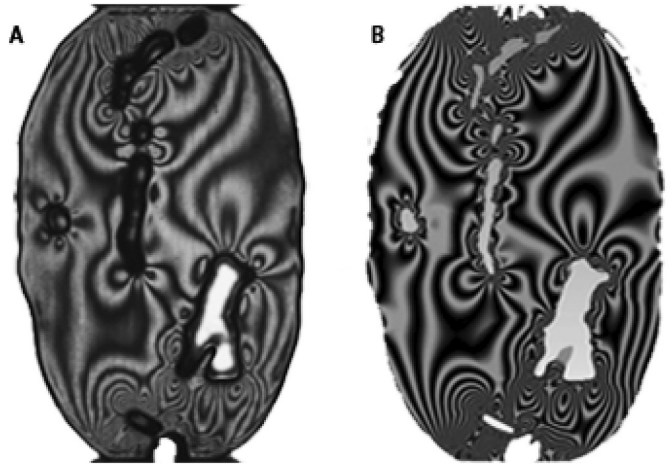

Fig. 14. Photoelastic response of the (A) 3D-printed digitally extruded cross-section of the coffee bean with internal voids and (B) FEA simulation, both to 0.25 mm displacement.

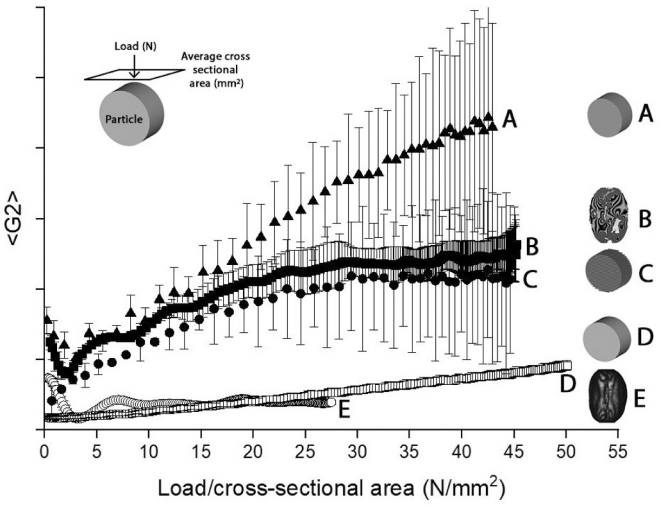

Fig. 15. The gradient-squared (G^2) approach was used to quantify the amount of light produced for the tested particles. The gradient squared light intensity plotted against the normalized force loads shown for the particles starting from top to bottom of the graph: 2D VeroClear disc – perpendicular print layers (A), 2D digitally extruded cross-section of coffee bean (B), 2D VeroClear disc – parallel print layers (C), 2D acrylic disc (D) and 3D solid coffee bean (E).

The G^2 value for the 3D coffee bean (Fig. 15E) with solid internals does not behave in the same way as the 2D particle shapes. An initial deviation in the G^2 value before it plateaus, which could be due to a lensing effect caused by the curved structure of the particle, as was reported above. However, the 2D extruded cross-section of the coffee bean displays a similar trend to the 3D-printed 2D disc shape. This effect suggests that the G^2 method can be applied to 3D-printed particles and is better suited for particles with a constant 2D cross-section. Additionally, the irregularity of the external and internal particle shapes is not a limitation of this method. To improve the method [9–11], the fully 3D particles should be observed in a bath containing an index-matched solution to avoid lensing effects.

The other notable aspect about Fig. 15 is the difference in the scale of the error bars around the average G^2 value for each sample. The VeroClear 3D-printed discs (A and C) and the 2D bean cross-section (B) all have quite significant variations in the G^2 value as a function of load per unit area. Unexpectedly, the 3D solid coffee bean (E) shows less variation about the G^2 value, even though this is by far the most complex shape tested. Although there is a lot of work yet to be done on improving both the experimental approach to photoelastic stress studies of complex particles as well as the theory of such complex refraction patterns, the low variation in the solid 3D coffee bean data is an encouraging sign that the stress response of complex 3D shapes will in future be easily understood in future.

The use of VeroClear as a printing material shows promise, in concert with the development of some additional techniques. Further work to develop its modelling should treat it as an anisotropic material and account for the rotation of polarization due to the material itself, beyond the superimposed photoelastic response. This would allow for more quantitative measurements than are presently possible. With this in place, 3D printing could be used to investigate the photoelastic stress visualization for complex particle geometries and particle assemblies, bringing researchers one step closer to being able to understand the behavior of and model the stress within complex geometries.

4. Conclusions

This study explored the feasibility of photoelastic stress measurements for various geometries of 3D-printed particles. For disc shapes, variations in the photoelastic properties were found due to the relative orientation of the print axis, particle axis, and compression axis. These changes occurred even though the mechanical properties were not significantly affected by the change in orientation of the print layer. In addition, a strong photoelastic response in more complicated 3D shapes was observed, although only a semi-quantitative interpretation was accessible.

We found that, due to mechano-optical artefacts from the printing process, the VeroClear material should be recalibrated to the specific print orientation for each specific particle fabrication. The FEA results modeled the regions of high and low stress, particularly around the internal voids, and the development of the stress fringes was in good agreement with the experimentally observed stress fringes. Intricate internal geometries within a complex 3D shape make the stress visualization difficult to quantify. The possibility of using a digitally extruded 2D cross-section of the complex coffee bean shape was explored, and significant differences compared to the fully 3D bean were found. Also reported, for the first time, the application of the G^2 method o 3D-printed particles of simple and complex geometries for semi-quantification of the internal stress. A linear trend was also produced for 2D circular and irregular shapes, although the complexity of 3D shapes, with or without internal voids, requires more sophisticated methods to be developed.

Supplementary data to this article can be found online at https://doi.org/10.1016/j.powtec.2022.117852.

CRediT authorship contribution statement

Negin Amini: Investigation, Methodology, Data curation, Formal analysis, Project administration, Writing - original draft. **Josh Tuohey:** Data curation, Writing – review & editing. **John M. Long:** Investigation, Supervision, Writing – review & editing. **Jun Zhang:** Methodology, Writing – review & editing. **David A.V. Morton:** Supervision, Writing – review & editing. **Karen E. Daniels:** Supervision, Formal analysis, Writing - review & editing. **Farnaz Fazelpour:** Writing - review & editing. **Karen P. Hapgood:** Conceptualization, Funding acquisition, Supervision, Writing – review & editing.

Declaration of Competing Interest

Karen Hapgood reports financial support was provided by IFPRI. Karen Hapgood reports financial support was provided by ARC Discovery Project. Karen Daniels reports financial support was provided by National Science Foundation.

Data availability

Data will be made available on request.

Acknowledgements

This work was supported by the International Fine Particles Research Institute (IFPRI) and an Australian Research Council (ARC) Discovery Project, grant DP150100119. Karen Daniels is grateful for support from the National Science Foundation, grant DMR-2104986. The authors would like to give thanks to Dr. Asadul Haque for assistance with X-ray Computed Tomography scans of the coffee bean at Monash University. We also thank Damian Elderfield for his assistance with processing 3D printing files at Deakin University.

References

[1] K. Ramesh, Developments in Photoelasticity, IOP Publishing, 2021.
[2] R.B. Barnes, L.G. Bonner, The Christiansen filter effect in the infrared, Phys. Rev. 49 (10) (1936) 732.
[3] T. Wakabayashi, Photo-elastic method for determination of stress in powdered mass, J. Phys. Soc. Jpn. 5 (5) (1950) 383–385.
[4] C.-H. Liu, et al., Force fluctuations in bead packs, Science 269 (5223) (1995) 513–515.
[5] D. Howell, R. Behringer, C. Veje, Stress fluctuations in a 2D granular Couette experiment: a continuous transition, Phys. Rev. Lett. 82 (26) (1999) 5241.
[6] A.A. Zadeh, et al., Enlightening force chains: a review of photoelasticimetry in granular matter, Granul. Matter 21 (4) (2019) 83.
[7] K.E. Daniels, J.E. Kollmer, J.G. Puckett, Photoelastic force measurements in granular materials, Rev. Sci. Instrum. 88 (5) (2017), 051808.
[8] R. Hurley, et al., Quantifying interparticle forces and heterogeneity in 3D granular materials, Phys. Rev. Lett. 117 (9) (2016), 098005.
[9] I. Zuriguel, T. Mullin, J. Rotter, Effect of particle shape on the stress dip under a sandpile, Phys. Rev. Lett. 98 (2) (2007), 028001.
[10] Y. Zhao, J. Bares, B. Behringer, How does particle shape affect the near jamming properties of granular materials? Pentagons vs. disks. APS 2016 (2016) (p. C43.008).
[11] D. Fischer, et al., Force chains in crystalline and frustrated packing visualized by stress-birefringent spheres, Soft Matter 17 (16) (2021) 4317–4327.
[12] W. Li, et al., Photoporomechanics: an experimental method to visualize the effective stress field in fluid-filled granular media, Phys. Rev. Appl. 16 (2) (2021), 024043.
[13] P. Yu, et al., Monitoring three-dimensional packings in microgravity, Granul. Matter 16 (2) (2014) 165–173.
[14] M. Meyer, et al., Particle systems for efficient and accurate high-order finite element visualization, IEEE Trans. Vis. Comput. Graph. 13 (5) (2007) 1015–1026.
[15] M. Cárdenas-Barrantes, et al., Micromechanical description of the compaction of soft pentagon assemblies, Phys. Rev. E 103 (6) (2021), 062902.
[16] J.F. Doyle, J.W. Phillips, D. Post, Manual on Experimental Stress Analysis, Soc. Exp. Mech. 5 (1989) 107–135.
[17] K.E. Daniels, N.W. Hayman, Force chains in seismogenic faults visualized with photoelastic granular shear experiments, J. Geophys. Res. Solid Earth 113 (B11) (2008).
[18] A.H. Clark, L. Kondic, R.P. Behringer, Particle scale dynamics in granular impact, Phys. Rev. Lett. 109 (23) (2012), 238302.
[19] K.E. Daniels, J.E. Coppock, R.P. Behringer, *Dynamics of meteor impacts.* Chaos: an interdisciplinary, J. Nonlinear Sci. 14 (4) (2004) S4.
[20] J. Krim, P. Yu, R. Behringer, Stick–slip and the transition to steady sliding in a 2d granular medium and a fixed particle lattice, Pure Appl. Geophys. 168 (12) (2011) 2259–2275.
[21] N. Iikawa, M.M. Bandi, H. Katsuragi, Structural evolution of a granular pack under manual tapping, J. Phys. Soc. Jpn. 84 (9) (2015), 094401.
[22] S. Lherminier, et al., Continuously sheared granular matter reproduces in detail seismicity laws, Phys. Rev. Lett. 122 (21) (2019), 218501.
[23] L. Wang, et al., The mechanical and photoelastic properties of 3D printable stress-visualized materials, Sci. Rep. 7 (1) (2017) 1–9.
[24] VeroClear Rigid Transparent Polyjet material, in: Stratasys (Ed.), 7665 Commerce Way, Eden Prairie, MN, 2018, p. 55344.
[25] Y. Ju, et al., Visualization of the complex structure and stress field inside rock by means of 3D printing technology, Chin. Sci. Bull. 59 (36) (2014) 5354–5365.
[26] J.P. Mathews, et al., A review of the application of X-ray computed tomography to the study of coal, Fuel 209 (2017) 10–24.
[27] D638-02a, A, Standard Test Method for Tensile Properties of Plastics, ASTM International West Conshohocken, 2002.
[28] Standard, A.D, Standard test method for compressive properties of rigid plastics, in: Annual Book of ASTM, 1996, pp. 78–84.
[29] L. Bass, N.A. Meisel, C.B. Williams, Exploring variability of orientation and aging effects in material properties of multi-material jetting parts, Rapid Prototyp. J. 22 (2016) 827–832.
[30] Technical Specifications of Acrylic Sheet, Available from: https://www.cutmyplastic.co.uk/acrylic-technical-specification/, 2019.
[31] Perspex® Cell Cast Acrylic Technical Data Sheet, Available from: https://www.allplastics.com.au/component/docman/doc_download/382-allplastics-perspex-cell-cast-acrylic-technical-data-sheet-en?Itemid, 2020.
[32] Y. Zhao, et al., Jamming transition in non-spherical particle systems: pentagons versus disks, Granul. Matter 21 (4) (2019) 1–8.